Available online at www.sciencedirect.com
SCIENCE DIRECT®
Journal of Nuclear Materials 335 (2004) 443–456
journal of nuclear materials
www.elsevier.com/locate/jnucmat

Oxidation kinetics of Zircaloy-4 and Zr–1Nb–1Sn–0.1Fe at temperatures of 700–1200°C

Jong Hyuk Baek *, Ki Bum Park, Yong Hwan Jeong

Zirconium Fuel Cladding Team, Korea Atomic Energy Research Institute, P.O. Box 105, Yuseong, Daejeon 305-600, South Korea

Received 22 April 2004; accepted 16 August 2004

Abstract

The oxidation characteristics for the Zircaloy-4 and Zr–1.0Nb–1.0Sn–0.1Fe alloys were investigated in the temperature ranges of 700–1200 °C for 3600 s under steam supply conditions, using a modified thermo-gravimetric analyzer. The oxidation at these temperatures generally complied with the parabolic rate law for the examined duration up to 3600 s. However, the parabolic rate was not obeyed in the temperature ranges of 800–1050 °C. The oxidation kinetics were changed depending on the oxidation temperatures due to the phase transformations of the base metal and its oxide. The oxidation rate exponents of the Zr–1.0Nb–1.0Sn–0.1Fe alloy at all the temperatures were higher than those of Zircaloy-4. Considering the data controlled by the parabolic rates at 700, 1100, 1150, and 1200 °C, the oxidation rate constants were the same slopes as the Baker–Just relationship. The rate transition at 800 °C could have resulted from the phase transformation of the base metal and those at 1000 and 1050 °C could have resulted from the lateral cracks in the oxide due to the ZrO_2 phase transformation from a monoclinic structure to a tetragonal structure.

PACS: 42.81.B; 81.65.M; 81.65.K

1. Introduction

The current trend in the nuclear industry is to increase the fuel discharge burn-up because of the major advantages in the fuel cycle cost, reactor operation, and spent fuel management. At a high burn-up, fuel rods fabricated from conventional Zircaloys often exhibit a significant degradation such as oxidation, hydriding and oxide spallation. Thus many fuel vendors have developed the advanced cladding materials, such as ZIRLO, M5, MDA, and NDA, for the high burn-up fuel to improve their safety and economical efficiency [1–5].

During a typical loss of coolant accident (LOCA) conditions, the fuel claddings are subjected to a high-temperature oxidation and finally quenched because of the reflooding of the core [6,7]. Since the 1960s, extensive studies were carried out to precisely evaluate the oxidation rate of Zircaloy in a high-temperature steam for a LOCA safety analysis [7–17]. The kinetics data showed a relatively good agreement with each other, though the kinetics by Baker–Just is generally considered to overestimate the reaction in the temperature range above 1000 °C. In most of the previous studies on Zircaloys, the oxidation rates were determined mainly in the

* Corresponding author. Tel.: +82 42 868 8823; fax: +82 42 862 0432/686 8346.
E-mail address: jhbaek@kaeri.re.kr (J.H. Baek).

0022-3115/$ - see front matter © 2004 Elsevier B.V. All rights reserved.
doi:10.1016/j.jnucmat.2004.08.007

temperature range above 1000 °C, while a limited number of studies were conducted in the temperature range from 600 to 1000 °C [18–23]. The oxidation kinetics at temperatures higher than 1000 °C generally complied with the parabolic rate [7–17]. But some researchers pointed out that the oxidation kinetics would not obey the parabolic rate in the temperature ranges below 1000 °C. Nagase et al. insisted that a cubic rate law was preferable for the oxidation below 980 °C and the discontinuities in the temperature dependency of the oxidation rate constant were observed due to the monoclinic/tetragonal phase structure change of the zirconium oxide [18]. Uetsuka and Hofman found that the oxidation reaction obeyed a cubic rate law at 900 °C, but a parabolic rate law at temperatures above 1000 °C [16]. Leistikow and Schanz studied the oxidation kinetics at the temperatures from 600 to 1300 °C. They insisted that the transition from a cubic or parabolic to a linear oxidation rate occurred by oxide scale cracking in the temperature ranges from 600 to 1000 °C, but at and above 1050 °C, no change in the rate law towards an accelerated oxidation was detected [19,20]. Westerman found that the oxidation obeyed a cubic rate law for the temperature range from 600 to 850 °C and provided the cubic rate law constant [21]. Pawel et al. also insisted that the oxidation kinetics between 900 and 1000 °C were a non-parabolic rate law [15,22]. S.M. Sathe et al. performed the oxidation testing for the temperatures from 650 to 1150 °C [23]. But they did not mention the oxidation behaviors in the temperature ranges of 800–1050 °C. The database regarding the oxidation kinetics at the temperatures below 1000 °C is not sufficient and the transition of the oxidation rate at these temperatures has not yet been sufficiently understood.

Furthermore, the data on the oxidation kinetics of the Nb-containing Zr alloys have not been published and are not easily found. A few studies on high-temperature oxidation were carried for advanced cladding materials [24,25]. In order to achieve a comprehensive assessment of the suitability of Zr–1Nb cladding, Bohmert et al. studied the high-temperature oxidation of Zr–1Nb and Zircaloy-4 in the temperature range from 700 to 1100 °C [24]. But they did not mention the transition of the oxidation kinetics in these temperature ranges.

In this study, therefore, the oxidation kinetics of Zircaloy-4 and the Zr–1.0Nb–1.0Sn–0.1Fe alloys were compared and investigated in detail in the temperature ranges of 700–1200 °C at the early stage shorter than 3600 s. In addition, the microstructures of the alloys were also characterized after the oxidation testing.

2. Experimental

Table 1 shows the chemical composition of the zirconium alloys used in this study. The apparatus for the high-temperature testing was established by modifying the Shimadzu TGA (Thermogravimetric Analyzer, TGA 51H) as shown in Fig. 1. A test specimen was freely hung from a Pt wire connected to TGA apparatus.

Table 1
Chemical composition of zirconium alloys

	Nb (wt%)	Sn (wt%)	Fe (wt%)	Cr (wt%)	Zr (wt%)
Zircaloy-4	–	1.35	0.2	0.1	Bal.
Zr–1.0Nb–1.0Sn–0.1Fe	1.0	1.0	0.1	–	Bal.

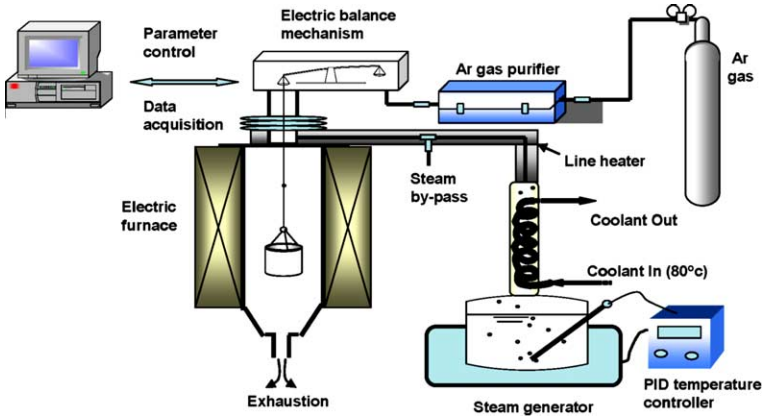

Fig. 1. Apparatus for the high-temperature oxidation testing.

The steam generator was attached to supply steam continuously into the furnace. The steam flow rate was controlled by the coolant temperature (80 ± 1 °C) of the attached condenser and established in a range (0.5–0.6 ml/min) not affecting the weighing accuracy of the electric balance due to the buoyancy effects. The weight change was measured by an in-suit method within ±0.001 mg during the oxidation reaction. And the temperature of the test specimen was controlled and measured accurately to within ±0.1 °C by a computer system. During the heat-up to the desired temperature and the oxidation test, high purity (99.999%) Ar gas was purged into the furnace at the flow rate of about 20 ml/min. The heating rate up to the desired temperature was set at 50 °C/min, and then the oxided sample after the oxidation test was cooled down to room temperature by an electric pan. The prepared steam together Ar as a carrier gas was supplied into the furnace right after the temperature arrived at the desired value.

The specimens for the high-temperature oxidation testing were cut off from the cladding tubes. The size of the specimens was 8 mm in length and both ends of the specimens were ground carefully by SiC 1200 emery paper to minimize the error during the oxidation. All the specimens were finally pickled in a solution of 5% HF, 45% HNO_3, and 50% H_2O. After the oxidation testing, the microstructures of all the specimens were observed by a polarized optical microscope.

3. Results and discussion

From the weight gain data acquitted directly from the TGA were the amount of absorbed oxygen ($W_{\text{oxygen absorbed}}$) during the oxidation reaction. The oxidation reaction of Zr or Zr alloys under the high-temperature steam condition could be described by the following equation.

$$\mathrm{Zr} + 2\mathrm{H_2O} \rightarrow \mathrm{ZrO_2} + 2\mathrm{H_2} \tag{1}$$

Most researches on high-temperature oxidation have assumed that the oxide thickness after the oxidation could increase with the square root of the oxidation time [7–17], so-called the parabolic rate law. In other words, the oxidation rate could be strongly dependent upon the temperature and time during the oxidation and the weight gain at the early stage could result from the oxygen diffusion through the oxide layer in accordance with the parabolic rate. The relationship between the weight gain and exposure time is as follows;

$$W^2_{\text{oxygen absorbed}} = K_{\mathrm{p}} \cdot t, \tag{2}$$

where K_{p} the parabolic rate constant ($mg^2/dm^4/s$) and t the exposure time (s).

In this study, the parabolic rate relationship between $W_{\text{oxygen absorbed}}$ and t is not followed in all temperature ranges of 700–1200 °C. The oxidation rate at the temperatures from 700 to 1200 °C could be changed depending on the oxidation temperatures. Therefore, it is possible to generalize the relationship between the weight gain and the exposure time by introducing the generalized rate constant, K_n.

$$W^n_{\text{oxygen absorbed}} = K_n \cdot t, \tag{3}$$

where K_n the oxidation rate constant ($(mg/dm^2)^n/s$) having the rate exponent of n and t the exposure time (s).

In order to obtain the rate exponent and rate constant (n and K_n), non-linear fittings were carried out using the function of $y = a \cdot x^b$ at each temperature. From Eq. (3), the rate exponent and rate constant can be represented like as $n = 1/b$. Fig. 2 shows the non-linear fitting results for Zircaloy-4 in the temperature range of 700–950 °C. In the case of the 700 °C, 900 °C and 950 °C oxidation tests, the experimental data was fitted well by the proposed function for 3600 s. In the 800 °C test, the proposed function followed well the raw data before the exposure time of 2400 s. But, the transition of the oxidation rate revealed after 2400 s at 800 °C. These rate transitions at 800 °C could have occurred at 2400 ± 10 s from the repeated tests of 5 times. As mentioned above, however, the rate transitions at 900 and 950 °C were not observed for the oxidation time of 1 h. The rate transition for Zircaloy-4 was typically developed at about 60 mg/dm^2 $W_{\text{oxygen absorbed}}$ at 700 °C steam oxidation. So, it could be acceptable that the rate transition occurred at only 800 °C, not at 700, 900, and 950 °C.

Leistikow and Schanz proposed that the rate transition in the 800–900 °C temperature range would occur by the hydrogen absorption [20]. But this proposal has not been supported by other researchers until now. In his another studies, oxide cracking (the so-called breakaway effect) would result in the transition from a cubic or parabolic to a linear oxidation rate in the temperature range from 600 to 800 °C and at 1000 °C [19].

The other results of the non-linear fitting for Zircaloy-4 in the temperatures ranges of 1000–1200 °C are represented in Fig. 3. The transition of the oxidation rate was revealed at the temperatures of 1000 °C and 1050 °C. The transition time at 1000 °C was shorter than that at 1050 °C. But the rate transition did not occur at temperatures above 1100 °C. As shown in the 1000 °C oxidation, the oxidation kinetics was changed from a cubic rate to a linear rate at the time of 1800 s.

The temperature region of the two phase ($\alpha + \beta$) Zr phase in the Zircaloys is known generally to be between 810 °C and 970 °C [26], which depends on the oxygen concentration in the matrix. And the phase diagram of the Zr–O binary system shows that ZrO_2 exhibits a phase transformation from a monoclinic to a tetragonal at about 1000 °C [27]. According to the oxidation behaviors in Fig. 3, the structure transformation of ZrO_2

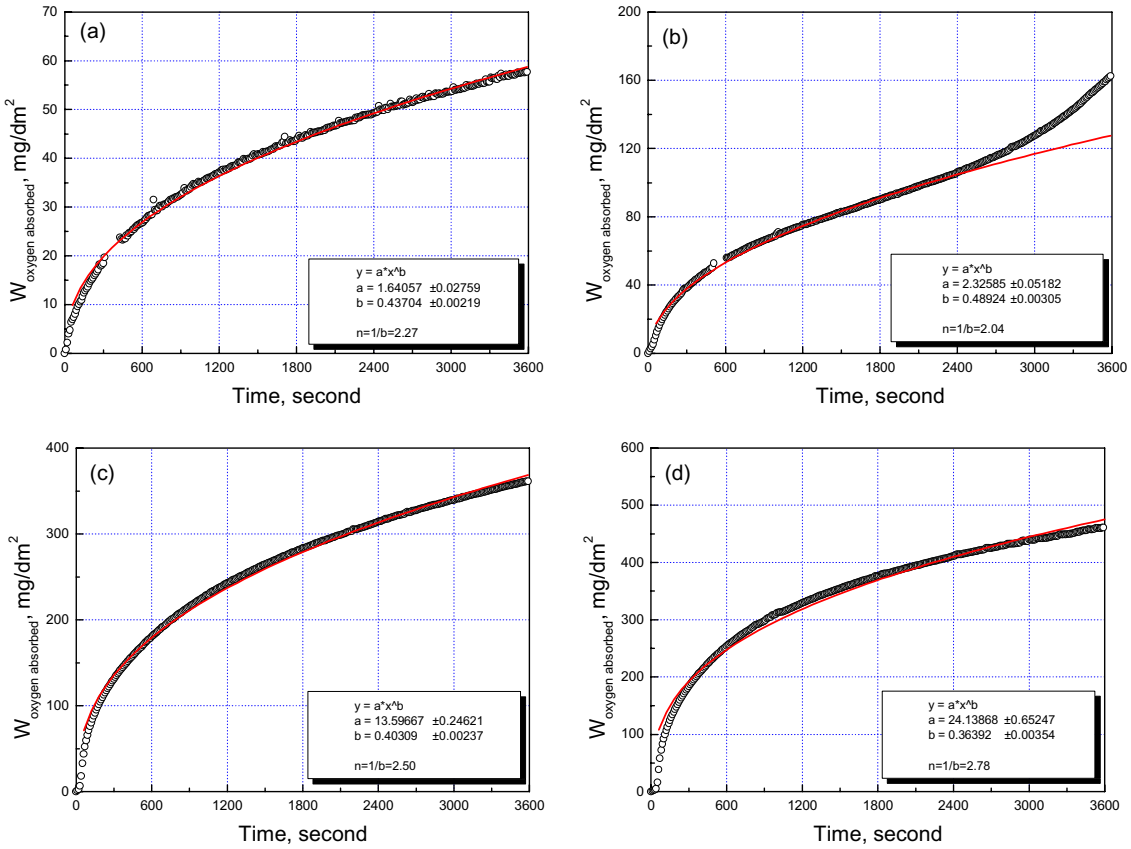

Fig. 2. Oxidation behaviors of the Zircaloy-4 at the temperatures of 700–950 °C; (a) 700 °C, (b) 800 °C, (c) 900 °C, (d) 950 °C.

would be processed in the temperature range from 1000 to 1050 °C. In other words, the two phases of monoclinic and tetragonal ZrO_2 would coexist within the temperatures of 1000–1050 °C. In this study, the rate transitions of Zircaloy-4 occurred at the temperatures from 900 to 1050 °C. It was possible to interpret the oxidation kinetics change from a cubic to a parabolic in the temperature range of 900–1050 °C. This agrees with Nagase's results of a gradual change of the oxidation kinetics between 900 and 1000 °C [18]. That is, the monoclinic and tetragonal phase structures of ZrO_2 within a temperature range would coexist and the relative proportion of the two phase structures would be changed with a temperature increase.

Fig. 4 shows the non-linear fitting results in the temperature range of 700 °C to 950 °C for the Zr–1.0Nb–1.0Sn–0.1Fe alloy. The proposed function of $y = a \cdot x^b$ followed well the experimental data for the 700, 900, and 950 °C oxidation. At 800 °C, however, the proposed function did not agreed with the experimental raw data after 2400 s. The transition of the oxidation kinetics occurred at that exposure time, which was almost the same exposure time as Zircaloy-4 in Fig. 2. Next the fitting of the experimental data at 1000–1200 °C for the Zr–1.0Nb–1.0Sn–0.1Fe alloy, the fitting results are represented in Fig. 5. As explained in the previous Fig. 3 for the Zircaloy-4, the transition of the oxidation rate for the Zr–1.0Nb–1.0Sn–0.1Fe alloy was also observed in the case of the 1000 °C and 1050 °C tests. The transition at 1000 °C occurred at a time of about 3200 s, while that at 1050 °C was 1900 s.

At 1000 °C in Figs. 3(a) and 5(a), the exposure time for the rate transition of the Zr–1.0Nb–1.0Sn–0.1Fe alloy was longer than that of Zircaloy-4. It is thought that this phenomenon could also be caused by the Nb addition in the Zr–1.0Nb–1.0Sn–0.1Fe alloy. The longer the rate transition lasted at the same oxidation temperature, the longer the cubic rate remained. Nb addition in the Zr alloy could make the ZrO_2 transformation temperature of the monoclinic to the tetragonal structure increase due to the Nb effect of the cubic kinetics stabilization. In short, the oxidation resistance of the Nb-containing Zr–1.0Nb–1.0Sn–0.1Fe alloy was better than that of Zircaloy-4 and the transition of the oxidation rate of the Zr–1.0Nb–1.0Sn–0.1Fe alloy was occurred at longer exposure time than Zircaloy-4.

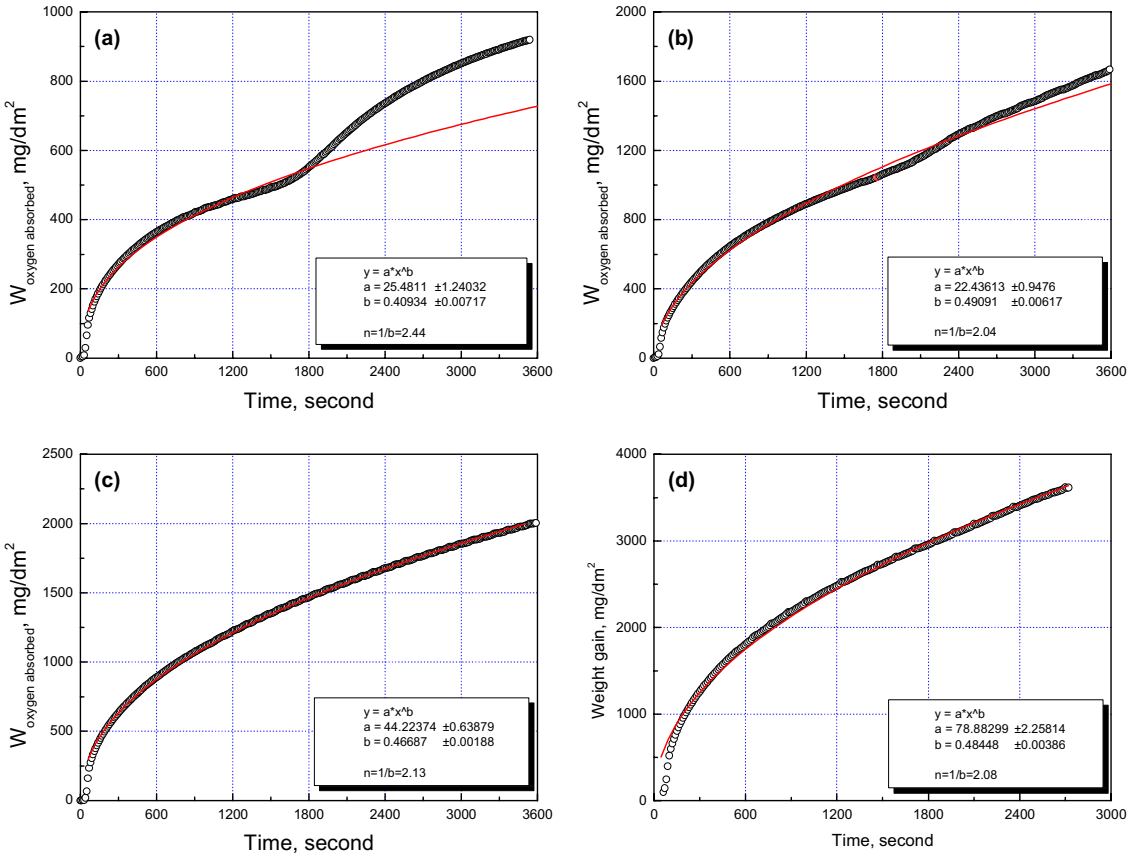

Fig. 3. Oxidation behaviors of the Zircaloy-4 at the temperatures of 1000–1200 °C; (a) 1000 °C, (b) 1050 °C, (c) 1100^o C, (d) 1200 °C.

Fig. 6 shows the variation of the rate exponent with the oxidation temperature for both alloys. In the case of Zircaloy-4, the rate exponent at 800 °C was relatively lower (n = 2.04) than that (n = 2.3–2.8) at the other temperatures (700 °C, 900 °C and 950 °C). The rate exponent was a maximum (n = 2.8) at 950 °C, and then was drastically reduced at temperatures above 1050 °C.

The lowest rate exponent at 800 °C could be explained by the mechanical property change of the base metal in the two phase region. The mechanical property change of the base metal in the two phase region would affect the stress relief in the oxide. It is thought that this would reduce the rate exponent at 800 °C. In the case of Zircaloy-4, 800 °C would be within the two phase ($\alpha + \beta$) Zr region. Thus the kinetics change at 800 °C after 2400 s could be caused by a moderate breakaway effect of the oxide. This could accelerate the oxidation rate at 800 °C. At the temperatures of 900 and 950 °C, the rate exponents were revealed by the cubic rate law. The oxidation kinetics could be changed gradually from a parabolic rate to a cubic rate as the oxidation temperature increased from 800 to 950 °C. Basically the reasons for the kinetic transition in these temperature ranges could be caused by the phase transformation of the base metal.

While, in the temperature range of 900–950 °C, the rate exponent of Zircaloy-4 increased with an increasing temperature, but in the ranges of 1000–1050 °C it was reduced as the temperature increased. The decrease of the rate exponent at 1000 and 1050 °C could be directly related to the transition of the oxidation rate. At the temperatures above 1100 °C, the rate exponent of Zircaloy-4 could not be adversely changed by varying the temperature. The oxidation kinetics of Zircaloy-4 were controlled by the parabolic rate at 1100–1200 °C. Therefore, it is thought that the oxidation rate should be changed at the ranges of 950–1050 °C from a cubic to a parabolic. This oxidation rate transition could be a result at 950–1050 °C from the change of the oxidation kinetics. Substantially, the oxidation kinetics changes in the temperature ranges of 950–1050 °C could originate from the crystal structure transformation of the zirconium oxide from a monoclinic to a tetragonal phase.

For Zircaloy-4, the oxidation kinetics changed with the temperature range of 700 °C to 1200 °C; parabolic

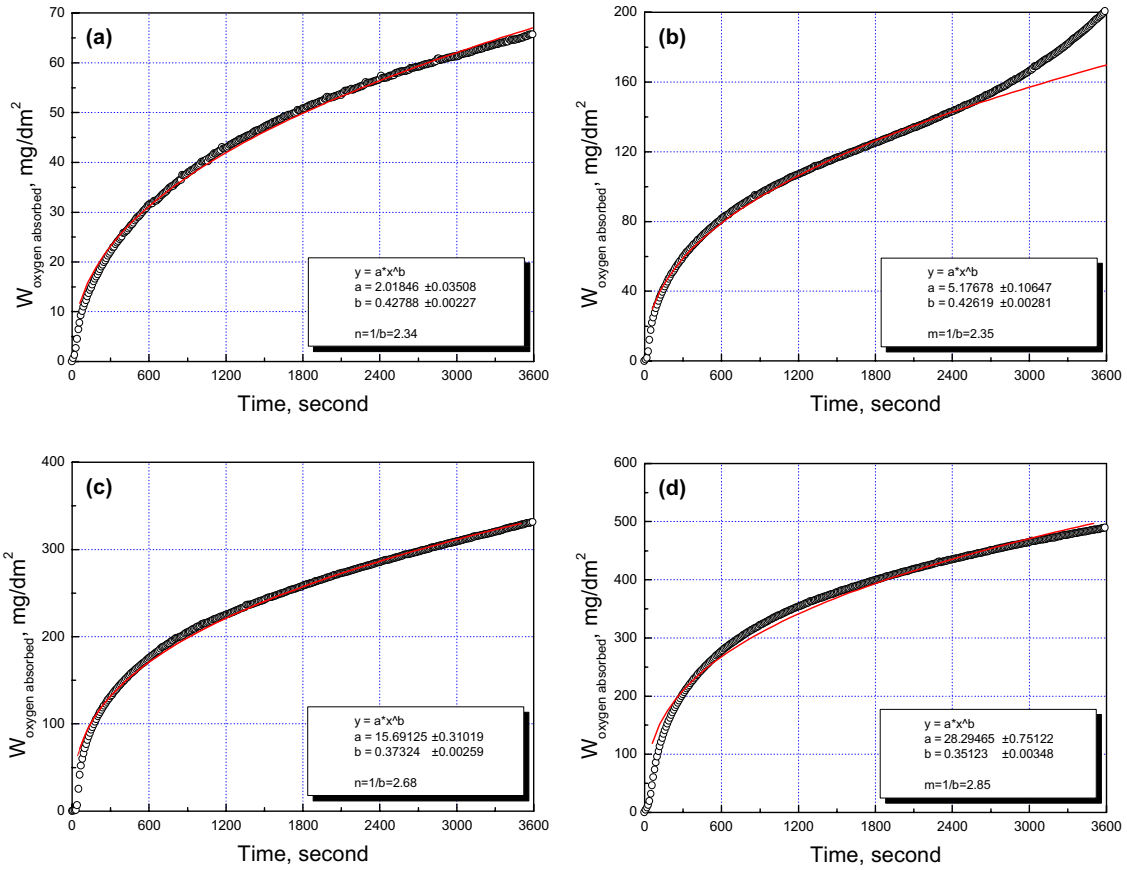

Fig. 4. Oxidation behaviors of the Zr–1.0Nb–1.0Sn–0.1Fe alloy at the temperatures of 700–950 °C; (a) 700 °C, (b) 800 °C, (c) 900 °C, (d) 950 °C.

rate (at 700 °C) → parabolic-linear rate (at 800 °C) → cubic rate (at 900–950 °C) → cubic-parabolic rate (at 1000 °C) → parabolic-linear rate (at 1050 °C) → parabolic rate (at 1100–1200 °C). The phase transformation of the base metal occurred at about 800 °C. The rate transition at 1000–1050 °C resulted from the ZrO_2 phase transformation from a monoclinic structure to a tetragonal structure. It was concluded that the kinetics transition at 800 °C and 1000–1050 °C resulted from the transformation of the base metal and the ZrO_2, respectively.

In Fig. 6, the variation trends of the rate exponents of the Zr–1.0Nb–1.0Sn–0.1Fe alloy were almost the same as those of Zircaloy-4. The rate exponent (n) of the Zr–1.0Nb–1.0Sn–0.1Fe alloy increased with an increasing temperature in the range of 700 °C to 950 °C. The kinetics of the Zr–1.0Nb–1.0Sn–0.1Fe alloy were changed by varying the temperatures; parabolic rate (at 700 °C) → parabolic-linear rate (at 800 °C) → cubic rate (at 900–950 °C). The rate exponent of the Zr–1.0Nb–1.0Sn–0.1Fe alloy at 1000 °C was still as high as 3.0. But the rate exponent at 1050 °C was rapidly reduced to 2.3. This means that the change of the oxidation kinetics started at 1000 °C and nearly ended at 1050 °C. At the temperatures above 1100 °C, the rate transition for the Zr–1.0Nb–1.0Sn–0.1Fe alloy was not detected and the rate exponents were in the range of 2.2–2.3. And the oxidation kinetics above 1100 °C agreed well with the parabolic rate. That is, the oxidation kinetics in the temperature ranges of 1000–1200 °C were changed; cubic-linear rate (at 1000–1050 °C) → parabolic rate (at 1100–1200 °C).

The absolute values for the Zr–1.0Nb–1.0Sn–0.1Fe alloy's rate exponents were relatively higher than those for Zircaloy-4. This means that the oxidation resistance of the Zr–1.0Nb–1.0Sn–0.1Fe alloy would be superior to that of Zircaloy-4 in all the temperature ranges. This could result from the difference in the chemical composition between the two alloys. It is thought that the Nb addition in the Zr alloy could improve the high-temperature oxidation resistance from the higher rate exponent.

When the Zr oxidation with steam occurred at the temperatures above 600 °C, the solid state reaction was

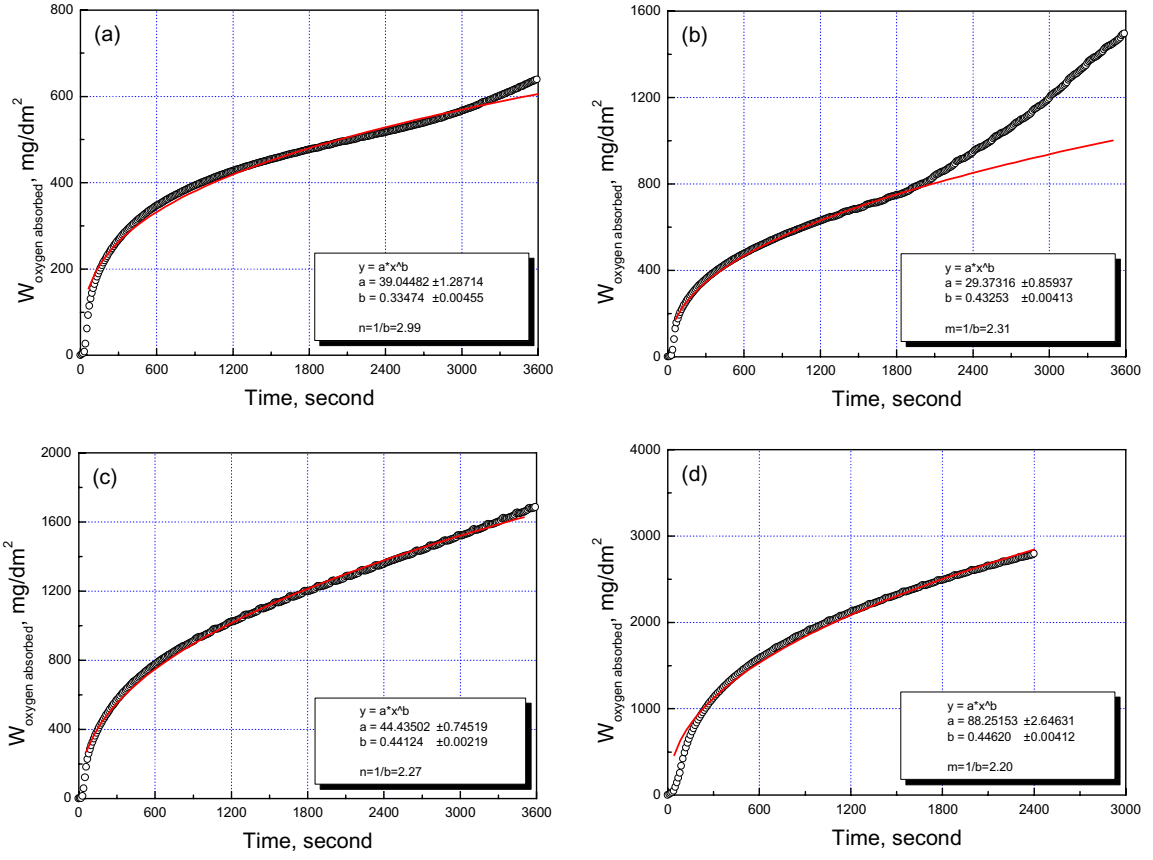

Fig. 5. Oxidation behaviors of the Zr–1.0Nb–1.0Sn–0.1Fe alloy at the temperatures of 1000–1200 °C; (a) 1000 °C, (b) 1050°C, (c) 1100 °C, (d) 1200 °C .

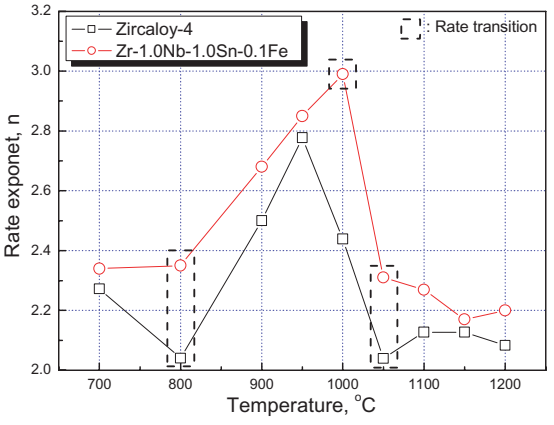

Fig. 6. Oxidation rate exponent of the zirconium alloys with the temperatures.

generally observed due to a deficiency of the oxygen ions within the ZrO_2 oxide layer. The rate constants during the oxidation were very dependent on the temperature. So

$$K_n = A \cdot \exp(-Q/RT), \tag{4}$$

where A is a constant $(mg/dm^2)^n/s)$, Q the activation energy for the oxidation reaction, R a universal gas constant (1.987 cal/mol K), and T the oxidation temperature (K).

From the rate exponents and rate constants (n and K_n) from Eqs. (3) and (4), it can be possible to estimate the $W_{\text{oxygen absorbed}}$ during the oxidation periods at specific temperatures. Fig. 7 represents the calculated $W_{\text{oxygen absorbed}}$ in comparison with the experimental $W_{\text{oxygen absorbed}}$ for both alloys after 3600 s at 700–1200 °C. When the rate transitions of Zircaloy-4 occurred at 800, 1000, and 1050 °C, the calculated weight gains (calculated $W_{\text{oxygen absorbed}}$) were underestimated but the other calculated weight gains agreed with the experimental values. For the Zr–1.0Nb–1.0Sn–0.1Fe alloy, the calculated weight gains at the temperatures of 800 and 1050 °C were also underestimated when compared to the experimental data. But the calculated $W_{\text{oxygen absorbed}}$ at 1000 °C was almost well expected for the experimental $W_{\text{oxygen absorbed}}$ because the rate transition occurred after 3200 s as described in Fig. 5(a).

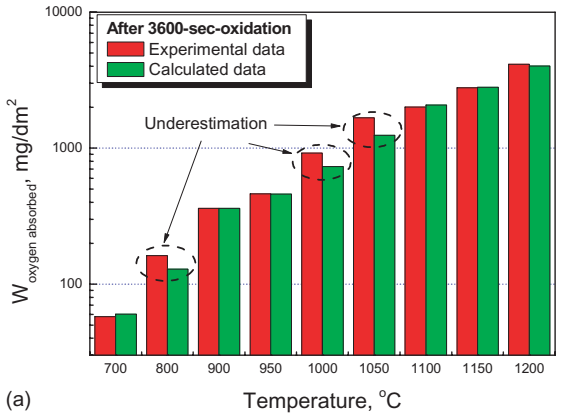

Fig. 7. Calculated $W_{\text{Zr-reacted}}$ from the analyzed oxidation rate; (a) Zircaloy-4 and (b) Zr–1.0Nb–1.0Sn–0.1Fe alloys.

Except for some cases of the oxidation rate transitions, the calculated rate exponents and rate constants were able to estimate exactly the experimental weight gains.

The Baker–Just relationship, which is obtained from the oxidation at temperatures above 1000 °C, has been used as the safety criteria of the high-temperature oxidation for the Zr cladding materials [8]. The oxidation rate constants for both alloys together with the Baker–Just relationship are shown in Fig. 8 with the inverse temperatures. The relationships between the rate constants and the temperatures for both alloys was obtained by ignoring some data (indicating as arrows in the Fig. 8) obtained at 800, 1000, and 1050 °C. The slops of the relationships for both alloys in this case are in accordance with that of the Baker–Just relationship but the rate constants of both alloys are higher than those of the Baker–Just relationship. The slops are the same because the parabolic rates could be controlled at the considered temperatures as in the Baker–Just relationship. It is necessary that the oxidation kinetics could not be obeyed by the parabolic rate law in the ranges of 900–1050 °C.

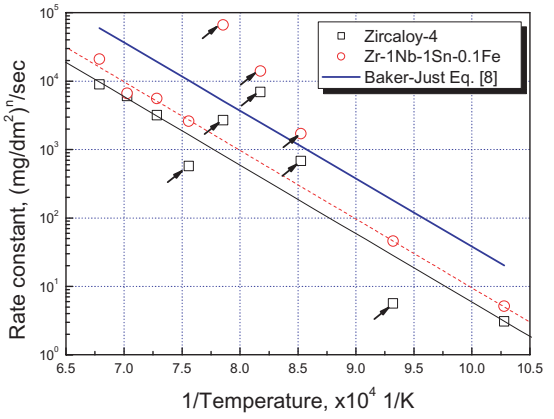

Fig. 8. Oxidation rate constant (K_n) of the zirconium alloys with the temperatures.

The surface appearances of the oxidized specimens were different depending on the test temperatures. After the oxidation for the same exposure time, the surface appearances for both the alloys are shown in Fig. 9. In the case of Zircaloy-4, the surface color at 700 °C was black and the color was changed into white yellowish gray with an increasing temperature up to 1050 °C. However, the surface color was recovered to a dark gray at the temperature of 1100 °C, and then above 1100 °C, the color tones were changed into white as the temperature increased. By glancing at the surface appearances, it is not difficult to see the discontinuities of the color tones at the temperatures of 800, 1000 and 1050 °C. These could be illustrated from the rate transitions during the oxidation. The rate transition could affect the oxidation kinetics and/or accelerate the oxidation rate. Then the accelerated rate of the oxidation could influence the discontinuities of ZrO_{2-x} non-stoichiometry and the surface color.

The trends of the surface color changes for the Zr–1.0Nb–1.0Sn–0.1Fe alloy in Fig. 9(b) were almost similar to those for Zircaloy-4. The color discontinuities of the Zr–1.0Nb–1.0Sn–0.1Fe alloy are also shown at the temperatures of 800, 1000 and 1050 °C. The rate transitions of the Zr–1.0Nb–1.0Sn–0.1Fe alloy occurred at these temperatures. It is concluded that the color discontinuities could be a result from the rate transitions during the oxidation testing.

Figs. 10 and 11 represents the microstructural changes for the Zircaloy-4 and Zr–1.0Nb–1.0Sn–0.1Fe alloys, respectively, by varying the oxidation temperatures from 700 °C to 1200 °C. The microstructures at 700 and 800 °C for Zircaloy-4, in Fig. 10, were α-Zr phase structures. The grains were coarsened with the temperature increase from 700 °C to 800 °C. At 950 °C, the microstructures consisted of two phases of α-Zr and β-Zr. The specimens oxidized at the temperatures

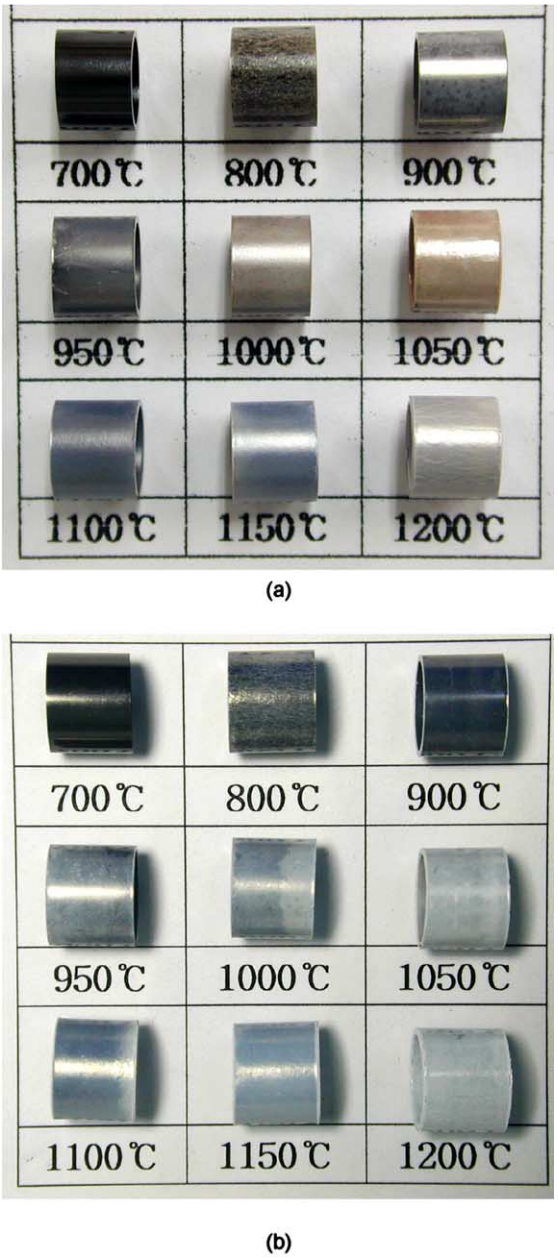

Fig. 9. Surface appearances of the alloys after the oxidation testing; (a) Zircaloy-4 and (b) Zr–1.0Nb–1.0Sn–0.1Fe alloys.

above 1000 °C had developed three layers; a zirconium oxide layer, an oxygen-stabilized α-Zr layer and a prior β-Zr layer with the depth from the outer surface. As the temperatures increased, the thickness of the oxygen-stabilized α-Zr layer was drastically increased and most of the prior β-Zr layer disappeared at 1200 °C. This is the reason why the diffusion depth of the oxygen was expanded with the increasing temperatures. And the thickness of the zirconium oxide layer was abruptly increased at 1050 °C. This abrupt change of the oxide thickness could have resulted from the rate transition of oxidation as already pointed out.

In the case of the Zr–1.0Nb–1.0Sn–0.1Fe alloy as shown in Fig. 11, the microstructures at the temperatures of the α-Zr and α + β Zr regions were different from those of Zircaloy-4. The grain growth of the Zr–1.0Nb–1.0Sn–0.1Fe alloy could be suppressed by the Nb addition in comparison with the grain size of Zircaloy-4 at the same temperature. The Nb addition in the Zr–1.0Nb–1.0Sn–0.1Fe alloy could also expand the region of the α + β Zr phase and then decrease at the starting temperature of the phase transformation of the base metal. Above 1000 °C, the microstructures of the Zr–1.0Nb–1.0Sn–0.1Fe alloy revealed the three-layer structures similar to those of Zircaloy-4. But the border between the oxygen-stabilized α-Zr layer and the prior β-Zr layer was not obvious in microstructures of the Zr–1.0Nb–1.0Sn–0.1Fe alloy. The oxygen-stabilized α-Zr phase was incorporated into the prior β-Zr phases. The mixed structures are obvious by the delayed diffusion rate of the Nb in the oxygen-stabilized α-Zr phases. The slower diffusion of Nb than oxygen could cause the oxygen-stabilized α-Zr phase to be incorporated into the prior β-Zr phase. The abrupt increase of the oxide thickness also occurred at 1050 °C for the Zr–1.0Nb–1.0Sn–0.1Fe alloy. This phenomenon could be interpreted from the viewpoint of the rate transition during the oxidation testing.

Fig. 12 provides the oxide microstructures for Zircaloy-4 to explain the microstructural changes at the temperature of the β-Zr phase. Many lateral cracks were contained within the oxide formed at 1050 °C but almost disappeared within the oxide at 1100 and 1200 °C. The lateral cracks would be evidence of the rate transition of oxidation kinetics. The crack formation within the oxide could be originally related to the ZrO_2 transformation from the monoclinic structure to the tetragonal structure. The oxide morphologies at 1100 and 1200 °C were changed into a columnar-like structure. This could also produce another trace of the tetragonal ZrO_2 during the oxidation at these temperatures [18]. The Sn segregation line was clearly observed within the oxide formed at 1200 °C. It has been reported that Sn could be concentrated in the line forming the compound of the Zr_4Sn due to the solubility and diffusion of the Sn in the zirconium oxide [28–30].

For the Nb containing Zr–1.0Nb–1.0Sn–0.1Fe alloy as shown in Fig. 13, a lot of lateral cracks were observed within the oxide formed at 1050 °C. But the lateral cracks were not found in the oxides at 1100 and 1200 °C. With a similar trend to Zircaloy-4, the oxide morphologies at 1100 and 1200 °C for the Zr–1.0Nb–1.0Sn–0.1Fe alloy were different from those at 1050 °C. The oxide morphologies at 1100 and 1200 °C were revealed with a columnar-like structure. It should be of

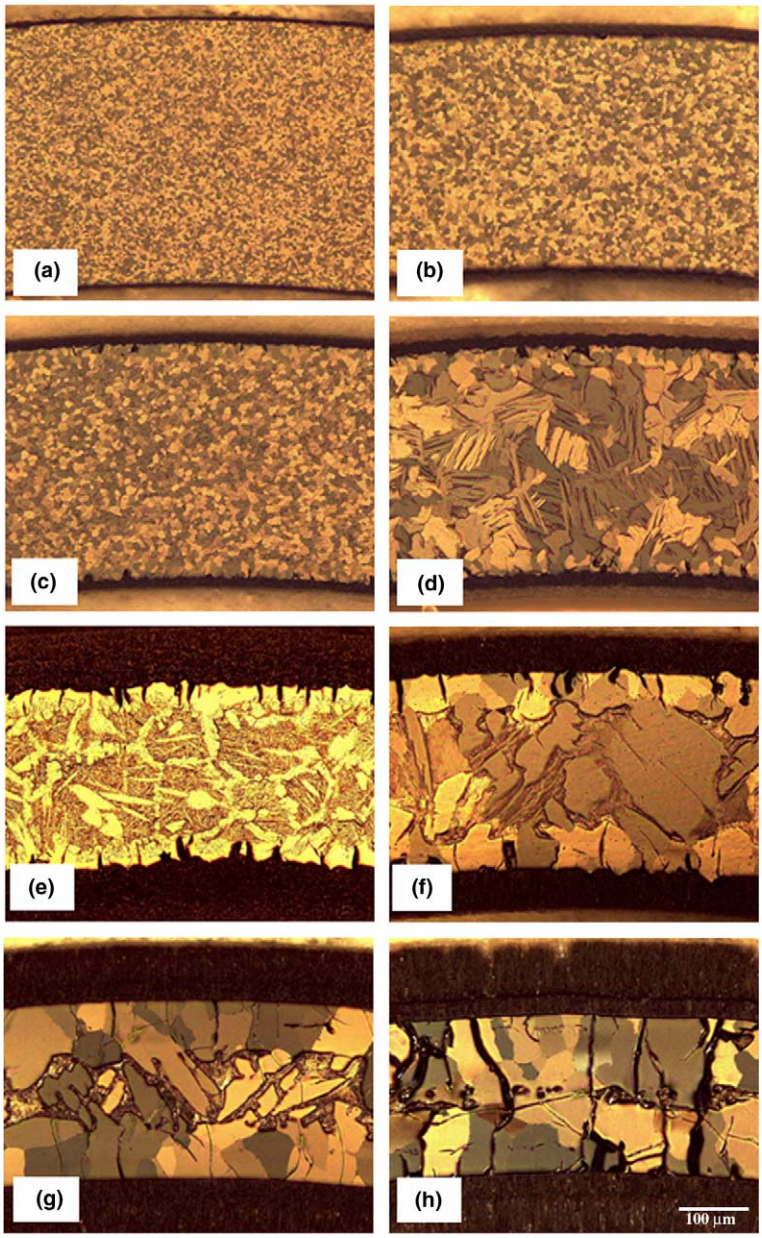

Fig. 10. Microstructural changes of the Zircaloy-4 with the oxidation temperatures; (a) 700 °C, (b) 800 °C, (c) 950 °C, (d) 1000 °C, (e) 1050 °C, (f) 1100 °C, (g) 1150 °C, (h) 1200 °C.

concern that there was no Sn segregation line within the oxide formed at 1200 °C in the case of the Zr–1.0Nb–1.0Sn–0.1Fe alloy. Perhaps, this could be related to the Nb addition into the Zr–1.0Nb–1.0Sn–0.1Fe alloy. Although the reason for this is not understood yet, the Nb addition in the Zr–1.0Nb–1.0Sn–0.1Fe alloy could prohibit the Sn segregation within the oxide. It is thought that the Nb addition could increase the Sn solubility within the oxide by stabilizing the tetragonal ZrO_2 phase.

On the basis of the previously described results and discussions, the oxidation characteristics of both alloys in the temperature ranges of 700–1200 °C are summarized in Fig. 14. According to the previous studies on standard Zircaloy-4 including 1.5 wt% Sn, the temperature range coexisting with the $\alpha + \beta$ Zr two phases in the zirconium-based alloy were found to have occurred between 810 and 970 °C at the equilibrium state [27]. But, it was assumed in this study that the transformation temperature from α-Zr to $\alpha + \beta$ Zr in this Zircaloy-4

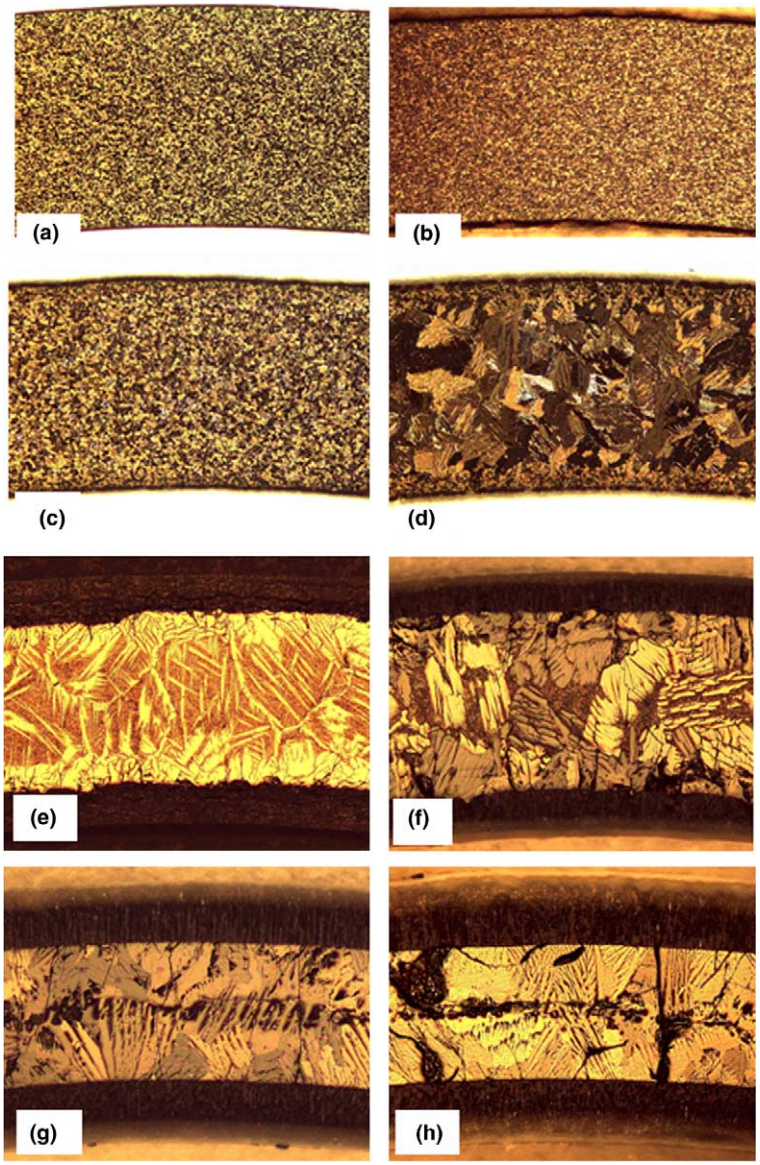

Fig. 11. Microstructural changes of the Zr–1.0Nb–1.0Sn–0.1Fe alloy with the oxidation temperatures; (a) 700 °C, (b) 800 °C, (c) 950 °C, (d) 1000 °C, (e) 1050 °C, (f) 1100 °C, (g) 1150 °C, (h) 1200 °C.

would be slightly changed by the decrease of the Sn contents (1.35 wt%). So, the transformation from the α-Zr to α + β Zr might have occurred at about 800 °C for Zircaloy-4. This phase transformation could result in a change of the oxidation kinetics from the parabolic rate to the parabolic-linear rate. It is thought that the rate transition could be revealed at 800 °C during the oxidation testing. And the rate exponent at 800 °C decreased when compared to that of the 700 °C. This could also have resulted from the change of the oxidation kinetics.

The crystal structure of the zirconium oxide could be transformed in the temperature range of 1000–1050 °C from a monoclinic to a tetragonal ZrO_2. Two phase oxides would be existed in the temperature region as shown in Fig. 14(a). It was deduced that the rate transition at 1000–1050 °C resulted from the structure transformation of the zirconium oxide. The oxidation kinetics was revealed by the cubic-parabolic rate and the cubic-linear at the temperatures between 1000 °C and 1050 °C. Especially, many lateral cracks were observed within the oxide formed at 1050 °C. It is thought that these cracks could be related to the oxidation rate transition due to the oxide structural change. The oxide thickness was abnormally increased at 1050 °C because of the formation

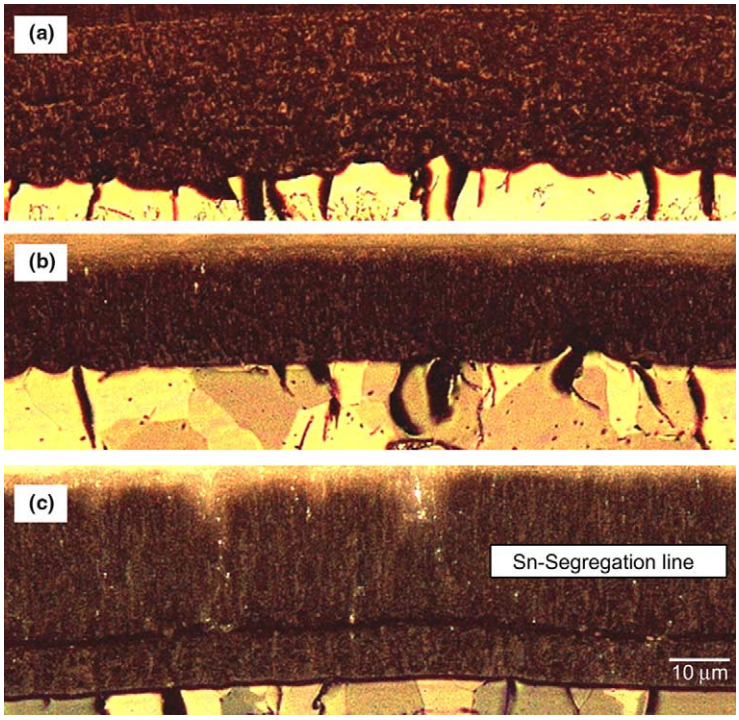

Fig. 12. Oxide morphologies of the Zircaloy-4 with the oxidation temperatures; (a) 1050 °C, (b) 1100 °C, (c) 1200 °C.

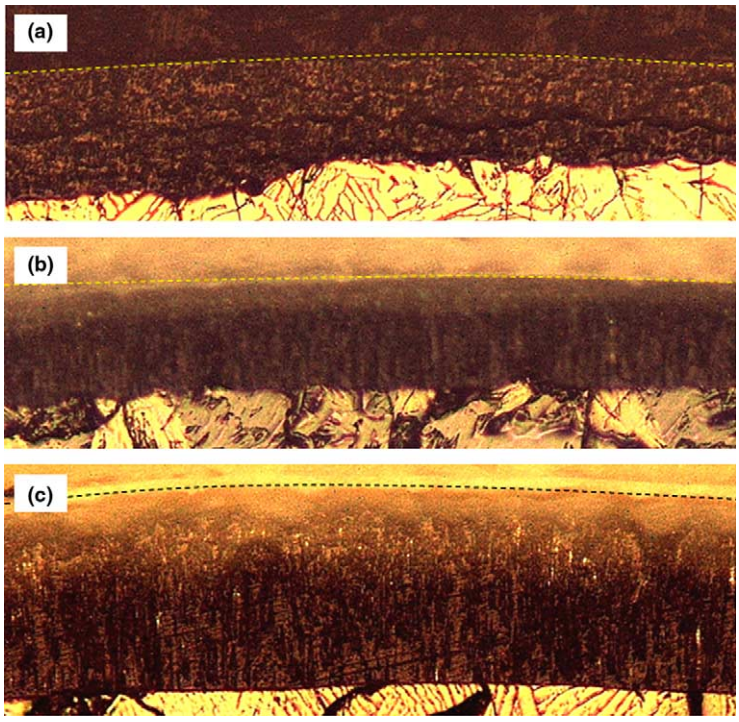

Fig. 13. Oxide morphologies of the Zr–1.0Nb–1.0Sn–0.1Fe alloy with the oxidation temperatures; (a) 1050 °C, (b) 1100 °C, (c) 1200 °C.

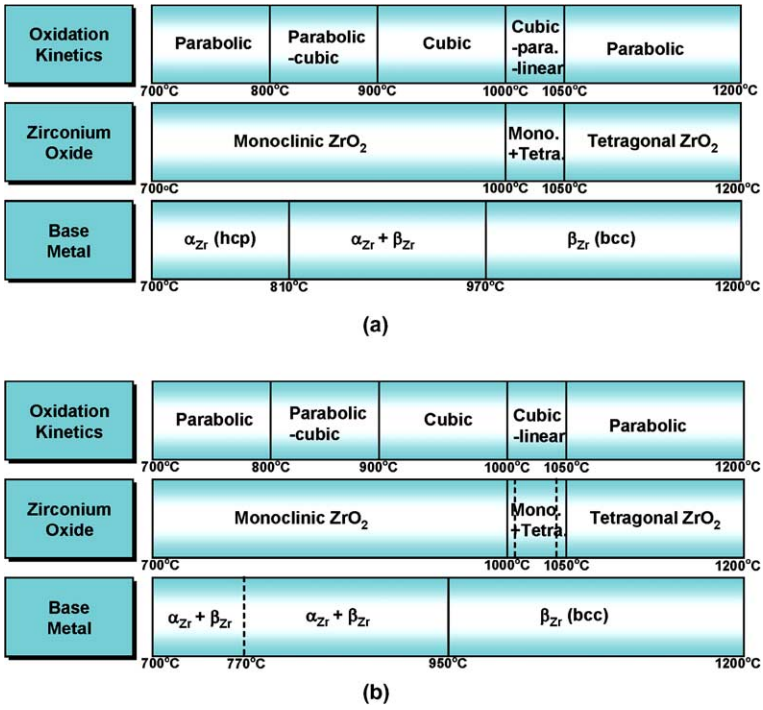

Fig. 14. Relationship between the oxidation kinetics and the phase range of the base metal and the zirconium oxide for; (a) Zircaloy-4 and (b) Zr–1.0Nb–1.0Sn–0.1Fe alloys.

of many lateral cracks. After the completion of the oxide structure transformation above 1100 °C, the oxidation kinetics would obey the parabolic rate law without the rate transition. As mentioned in Fig. 6, the rate exponents at 1100–1200 °C were nearly 2.1. The oxidation kinetics of Zircaloy-4 would be expected to be the parabolic rate above the transformation temperature of the oxide structure.

In the case of the Zr–1.0Nb–1.0Sn–0.1Fe alloy as shown in Fig. 14(b), the transformation temperatures of the base metals could be changed due to the Nb addition into the Zr–1.0Nb–1.0Sn–0.1Fe alloy. In general, the transformation from α-Zr + β-Nb to α-Zr + β-Zr would occur at around 610 °C for the Nb-containing Zr alloys [31,32]. But the massive transformation from α-Zr + β-Nb to α-Zr + β-Zr for the Zr–1.0Nb–1.0Sn–0.1Fe alloy would be at about 770 °C. And the completion temperature of the phase transformation for the Zr–1.0Nb–1.0Sn–0.1Fe alloy would be brought down due to the Nb addition in comparison to the Zircaloy-4. The massive phase transformation at 800 °C could influence the rate transition during the oxidation testing and then alter the oxidation kinetics to be the parabolic-linear rate. This trend for the Zr–1.0Nb–1.0Sn–0.1Fe alloy was the same as Zircaloy-4. The rate transitions and crack formation at 1000 and 1050 °C for the Zr–1.0Nb–1.0Sn–0.1Fe alloy could be deduced from the transformation of the zirconium oxide from a monoclinic to a tetragonal ZrO_2. These phenomena would also be affected by the change of oxidation kinetics.

By excluding some of the experimental data (indicating an arrow in Fig. 8) having the transition of the oxidation kinetics, the rate constants (K_n) for the Zircaloy-4 and Zr–1.0Nb–1.0Sn–0.1Fe alloy were put on the same fitting line and parallel to the Baker–Just relationship. The rate constants with parabolic-like rates at 700, 1100, 1150, and 1200 °C could be applied to the hypothesis of a parabolic rate law. It is recommended that the rate constants in the temperature ranges from 800 °C to 1050 °C should be reconsidered in the evaluation of the oxidation kinetics of the zirconium alloys. The parabolic rate law was not allowed at the temperatures of 800–1050 °C due to the change of the oxidation kinetics. In summary, the oxidation kinetics of the Zr-based alloys could be changed by the transformation of the base metal phases and oxide structures. Because the parabolic rate was not applied in the transformation temperature ranges, it is necessary that the rate constants for the zirconium alloys be reevaluated systematically in the temperature ranges of 800–1050 °C.

4. Conclusions

The oxidation kinetics was changed by varying the oxidation temperatures due to the phase transformations

of the base metal and its oxide; parabolic rate (at 700 °C) → parabolic-linear rate (at 800 °C) → cubic rate (at 900–950 °C) → cubic (or parabolic) linear rate (at 1000–1050 °C) → parabolic rate (at 1100–1200 °C). As a result of the transformations of the base metal and its oxide, the transitions of the oxidation rates were observed at 800, 1000, and 1050 °C for both the Zircaloy-4 and Zr–1.0Nb–1.0Sn–0.1Fe alloys. The discontinuity of the surface color change was in accordance with the oxidation rate transition at 800, 1000, and 1050 °C. And the oxidation resistance of the Zr–1.0Nb–1.0Sn–0.1Fe alloy at all the temperatures was superior to that of Zircaloy-4 from the higher rate exponent due to the Nb addition. Considering the data controlled by the parabolic rates at 700, 1100, 1150, and 1200 °C, the rate constants were on the same line for each alloy and they were the same slope as the Baker–Just relationship. The lateral cracks within the oxide formed at 1000–1050 °C were observed for both alloys because of the structural transformation from a monoclinic to a tetragonal ZrO_2. In this study, it was found that the parabolic rate was not controlled in the transformation temperature ranges of 800–1050 °C.

Acknowledgments

This study was supported by Korea Institute of Science and Technology Evaluation and Planning (KISTEP) and Ministry of Science and Technology (MOST), Korean government, through its National Nuclear Technology Program.

References

[1] G.P. Sabol, R.J. Comstock, R.A. Weiner, P. Larouere, R.N. Stanutz, ASTM STP 1245 (1994) 724.
[2] J.-P. Mardon, D. Chaquet, J. Senevat, ASTM STP 1354 (2000) 505.
[3] T. Isobe, Y. Matsuo, ASTM STP 1132 (1991) 346.
[4] T. Harada, M. Kimpara, K. Abe, ASTM STP 1132 (1991) 368.
[5] Y. Etoh, S. Shimada, T. Yasuda, T. Ikeda, R.B. Adamson, J.-S. Fred Chen, Y. Ishii, K. Takai, ASTM STP 1295 (1996) 825.
[6] F.J. Ebacher, S. Leistikow, ASTM STP 939 (1987) 451.
[7] G. Hache, H.M. Chung, Supporting paper presented during the Water Reactor Safety Meeting, Washington USA, 2000, NEA/CSNI/R, 2001, p. 18.
[8] L. Baker, L.C. Just, ANL-6548, 1962.
[9] H.M. Chung, G.R. Thomas, ASTM STP 824 (1984) 793.
[10] H. Ocken, R.R. Biederman, C.R. Hann, R.E. Westerman, ASTM STP 681 (1979) 541.
[11] V.F. Urbanic, T.R. Heidrick, J. Nucl. Mater. 75 (1978) 251.
[12] J.V. Cathcart, ORNL/NUREG?TM-41, 1976.
[13] A.F. Brown, T. Healey, J. Nucl. Mater. 88 (1980) 1.
[14] R.G. Ballinger, W.G. Dobson, R.R. Biederman, J. Nucl. Mater. 62 (1976) 213.
[15] R.E. Pawel, J.V. Cathcart, R.A. Mckee, J. Electrochem. Soc. Technol. 126 (7) (1979) 1105.
[16] Uetsuka, P. Hofman, J. Nucl. Mater. 168 (1989) 47.
[17] S. Kawasaki, T. Furuta, M. Suzuki, J. Nucl. Sci. Technol. 15 (8) (1978) 589.
[18] F. Nagase, T. Otomo, H. Uetsuka, J. Nucl. Sci. Technol. 40 (4) (2003) 213.
[19] S. Leistikow, ASTM STP 824 (1984) 763.
[20] S. Leistikow, G. Schanz, Nucl. Eng. Des. 103 (1987) 65.
[21] R.E. Westerman, J. Electrochem. Soc. 111 (1964) 140.
[22] R.E. Pawel, J.V. Cathcart, J.J. Cambell, J. Nucl. Mater. 82 (1979) 129.
[23] S.M. Sathe, V. Sethumadhavan, S. Kumar, D.N. Sah, Proceedings of the Symposium zirconium-2002 [ZIRC-02], 11–13 September 2002, Bhabha Atomic Research Center, Mumbai, India, 2002.
[24] J. Bohmert, M. Dietrich, J. Linek, Nucl. Eng. Des. 147 (1993) 53.
[25] V.I. Solyanyj, Yu.K. Bibilashvili, V.V. Dranenko, A.Ya. Levin, L.B. Izrajlevskij, A.M. Morozove, CONF-8404231, 1984.
[26] H.M. Chung, T.F. Kassner, J. Nucl. Mater. 84 (1979) 327.
[27] V.F. Urbanic, ASTM STP 633 (1977) 168.
[28] J.T. Prater, E.L. Courtright, ASTM STP 939 (1987) 489.
[29] R.E. Pawel, R.A. Perkins, R.A. Mckee, J.V. Cathcart, G.J. Yurek, R.E. Druschel, ASTM STP 633 (1977) 199.
[30] W.G. Dobson, R.R. Biederman, R.G. Ballinger, ASTM STP 633 (1977) 150.
[31] B.A. Rogers, D.F. Atkins, Trans. AIME 203 (1955) 1034.
[32] C.E. Lundin, R.H. Cox, Interim Report No.1, Contract No. At(11-1)-752, TID-11019, 1960.